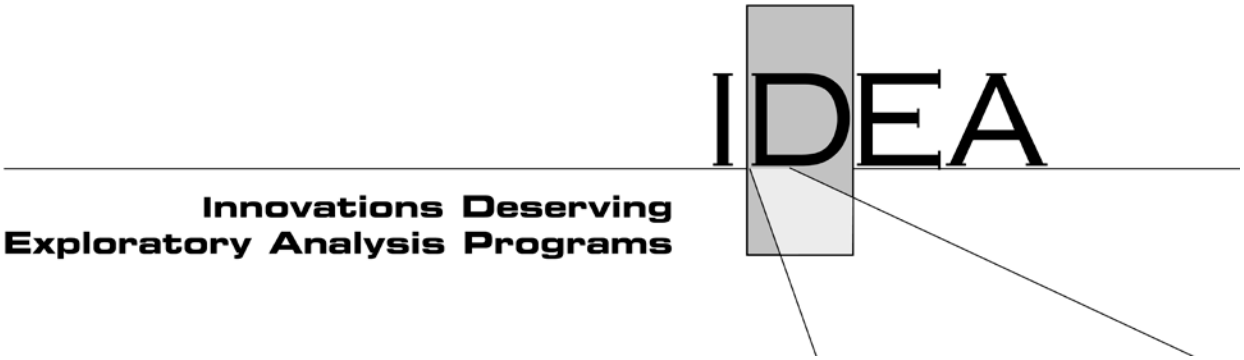

Rail Safety IDEA Program

Onboard High-Bandwidth Fiber-Optic Sensing System for Broken Rail Detection

Final Report for
Rail Safety IDEA Project 36

Prepared by:
Dr. Vahid Sotoudeh and Dr. Richard J. Black
Intelligent Fiber Optic Systems Corporation (IFOS)

November 2020

TRB TRANSPORTATION RESEARCH BOARD
The National Academies of
SCIENCES · ENGINEERING · MEDICINE

Innovations Deserving Exploratory Analysis (IDEA) Programs Managed by the Transportation Research Board

This IDEA project was funded by the Rail Safety IDEA Program.

The TRB currently manages the following three IDEA programs:

- The NCHRP IDEA Program, which focuses on advances in the design, construction, and maintenance of highway systems, is funded by American Association of State Highway and Transportation Officials (AASHTO) as part of the National Cooperative Highway Research Program (NCHRP).
- The Rail Safety IDEA Program currently focuses on innovative approaches for improving railroad safety or performance. The program is currently funded by the Federal Railroad Administration (FRA). The program was previously jointly funded by the Federal Motor Carrier Safety Administration (FMCSA) and the FRA.
- The Transit IDEA Program, which supports development and testing of innovative concepts and methods for advancing transit practice, is funded by the Federal Transit Administration (FTA) as part of the Transit Cooperative Research Program (TCRP).

Management of the three IDEA programs is coordinated to promote the development and testing of innovative concepts, methods, and technologies.

For information on the IDEA programs, check the IDEA website (www.trb.org/idea). For questions, contact the IDEA programs office by telephone at (202) 334-3310.

IDEA Programs
Transportation Research Board
500 Fifth Street, NW
Washington, DC 20001

Onboard High-Bandwidth Fiber-Optic Sensing System for Broken Rail Detection

IDEA Program Final Report

For the period 08/2018 through 11/2020

Contract No. SAFETY-36

Prepared for the IDEA Program

Transportation Research Board

National Academies of Sciences, Engineering, and Medicine

Dr. Vahid Sotoudeh and Dr. Richard J. Black
Intelligent Fiber Optic Systems Corporation (IFOS)
November 30, 2020

Acknowledgments

The IFOS team acknowledges the support of TRB funding through IDEA Contract No. SAFETY-36, and the very helpful contributions and support of the TRB Program Manager, Dr. Velvet Basemera-Fitzpatrick throughout the project. In addition, the team is particularly grateful to the project expert review panel members Mr. Tom Bartlett, Dr. Todd Snyder, Mr. John Zuspan and Dr. David Krohn as well as the reviewers on the oversight committee for all their insightful contributions and comments that helped improve this report.

Glossary

AAR	American Association of Railroads
CWT	Continuous Wavelet Transform
DPU	Data Processing Unit
FBG	Fiber Bragg Grating
FO	Fiber Optic
IF	Intensity Factor
NDT	Non-Destructive Testing
SNR	Signal-to-Noise-Ratio

Table of Contents

Investigator Profile

Principal Investigator: Dr. Richard J. Black, Chief Scientist at IFOS, obtained a B.Sc.(Hons.) in physics from the University of Canterbury, New Zealand, and a Ph.D. from the Research School of Physical Sciences at the Australian National University in optical fibers. He was a Research Fellow at the Ecole polytechnique de Montreal, Canada and was Invited Professor at the EPFL, Switzerland. He has made significant contributions in photonics (optical waveguide modes and modal interferometric devices) with application initially to telecommunications and then to optical fiber sensing for aeronautics, robotics, tranportation and structural health monitoring. Dr. Black is a Senior Member of AIAA and IEEE, and Life Member of ACM, OSA, SPIE and ASM International and Member of ACS.

Co-Principal Investigator: Dr. Sotoudeh, Product Director at IFOS, obtained his M.S. and Ph.D. from Stanford University. He has developed novel instrumentation and digital signal processing techniques for ambient and strong motion (earthquake) structural vibration measurement and analysis for system identification purposes. In collaboration with Stanford University and USGS, he organized and performed full-scale structural vibration tests on a series of buildings in the San Francisco Bay Area including buildings with unique suspended floor systems.

Intelligent Fiber Optic Systems Corporation, IFOS, headquartered in a Silicon Valley develops and sells advanced photonic and optoelectronic sensing products and solutions using fiber optics for the measurement and analysis of physical, chemical and biological parameters. Strains as small as sub micro-strain and as large as 10,000 micro-strain, vibrations, temperatures to 1000°C, pressures to 1 kBar, angular rates, magnetic fields, and a number of other parameters can be measured accurately at sampling rates in the kS/s to MS/s range simultaneously across large numbers of sensors in various operating environments and applications. Applications of IFOS sensor systems include protecting high-value assets in the transportation (e.g., rail), aerospace, energy and medical sectors.

Project Participants

TRB Program Manager:
Velvet Basemera-Fitzpatrick, PhD, PMP
Program Manager, Transit IDEA & Rail Safety IDEA
Transportation Research Board

P.I. + Team:
IFOS: Richard J. Black (PI), Vahid Sotoudeh, Behzad Moslehi, William Price
Adam Cheng, Levy Oblea
V3T (Subcontractor): Saied Taheri

Expert Review Panel:

Tom Bartlett	Automated Railroad Maintenance Systems (ARMS)
Todd Snyder	Amsted Rail
John Zuspan	Track Guy Consultants
David Krohn	Light Wave Venture

Executive Summary

There is a need for novel, technology-based sensing systems and analytic methods for monitoring and improving transportation rail safety through enhanced understanding of system and component failure modes, drivers, and timing. For example, one critical need is early-stage pre-catastrophic-failure detection of rail breakage, or emerging faults under trains. While these may not lead to immediate derailment until further damage occurs at the evolving rail fracture locations, it is critical that (1) such breakages or faults be detected and (2) an alert regarding their existence be sent before catastrophic damage or derailment does occur.

The objective of this TRB project was to develop an innovative onboard real-time broken rail and defect monitoring and detection system based on fiber-optic (FO) sensing technology that enables early-stage fault detection and repair well before the rail has reached a state which could lead to catastrophic derailment.

During our R&D work on this project at IFOS, the research team explored the broadband and high-speed capabilities of our advanced optical fiber Bragg grating (FBG) sensing and optoelectronic interrogation technology to enable real-time high-speed measurements of dynamic strain, shock, and vibration signals as well as their wideband spectral signatures as indicators of rail integrity (health) condition, both reliably and autonomously, in real time including while the train is in motion. The work has been approached with four technical tasks: (1) Design FBG sensor array in conjunction with data collection hardware and application-specific data analytics software. (2) Test onboard high-bandwidth FO sensor system in simulated broken rail condition scenarios. (3) Develop customized application-specific condition monitoring algorithms for broken rail detection. (4) Perform computer simulations of the train- rail system.

In this project the team defined, designed and performed lab tests to demonstrate the capability of IFOS' high-speed broadband FO sensing system in detecting the simulated event of the train wheel hitting a breakage point in the rail. In collaboration with the project subcontractor, V3T, the team developed signal processing algorithms to process the onboard FBG sensor data and identify rail break events on track. The team performed analytical work on studying the effect of noise, including the background acoustics and wheel-flats on the capability of the real-time FO sensing system in detecting the rail break events.

This project resulted in proof-of-concept of pre-catastrophic-failure rail breakage detection capability with high spatial and temporal resolutions (on the order of 1 mm at 65 mph train speed), and excellent sensing accuracy at high monitoring speeds (order of 1 mega-samples per second or 1 MS/s, per sensor).

IFOS' proposed onboard FO sensing system provides the enabling capability to detect rail breakage where other inspection tools such as non-destructive testing (NDT), hand-held inspection, visual inspection, and signaling are unavailable, and/or impractical, and/or labor intensive, and/or of limited value.

The system can augment existing track circuit-based broken rail detection and complement ultrasonic testing. For optimal protection, the system should be installed on a data processing unit on the rear of the train. In non-signaled territory, the system can far exceed the performance of the existing methodology of visual inspection.

IDEA Product

The product resulting from this IDEA program was a proof-of-concept of RailSense™, an innovative, onboard broken rail and defect detection system that utilizes IFOS' high-speed, low-noise, high-sensitivity broadband fiber Bragg grating (FBG) sensing technology comprising multifunctional, electromagnetic interference (EMI) immune FBG sensors and I*Sense® FBG sensor interogators (operating up to megasamples-per-second) together with signal processing algorithms allowing the extraction of broken rail signals from signals that could include wheel-flat signatures and environmental noise. The on-train RailSense system would typically be installed on a DPU located at the rear of the train and enable autonomous multi-functional real-time measurement of strain, shock, and vibration signals as indicators of rail condition while the train is in motion. The system has been designed to avoid false positives, and also has spin-off application to on-track measurements.

This broken rail detection methodology improves on the existing methodology, including track circuits (which detect rail that has already broken [1]) and ultrasonic testing (which detects probable locations of future broken rail, but has some current limitations for high-speed [2]) as well as visual inspection (the exisiting methodology for non-signaled territory).

Concept and Innovation

There is a need for novel, technology-based, reliable techniques for improving rail safety through enhanced understanding of system and component failure modes, drivers, and timing. Rail breaks [1, 3, 4] and wheel flats [5-10] are major problems for railway systems that require early detection for timely corrective actions. Detection of rail breakage under trains that does not lead to immediate derailment until further damage occurs at the fracture meets this need. Figure 1 gives an idea of the percentage of potential rail breaks that are detected by different inspection tools - see [11], which also details the different types of rail degradation which leads to cracks and ultimately rail breakage.

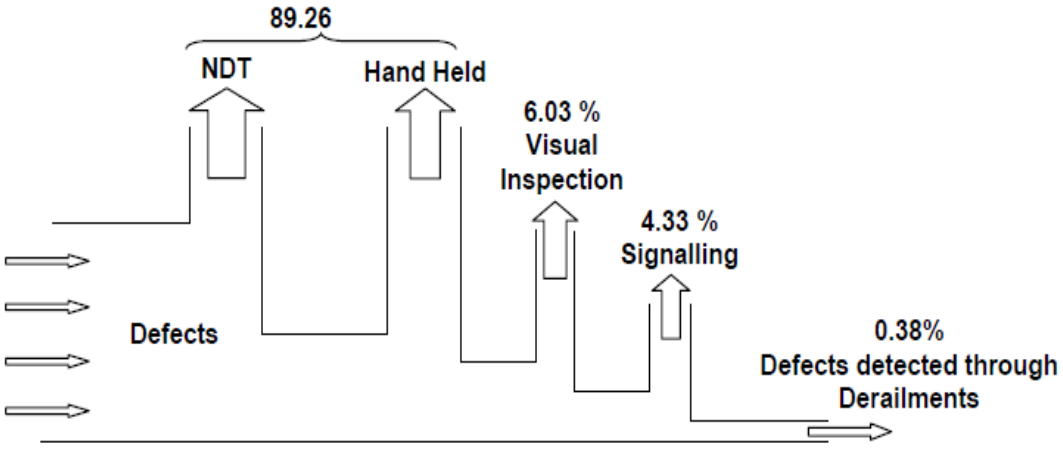

Figure 1: Percentage of potential rail breaks detected from different inspection tools [11].

Concept

The IFOS system exploits the broadband and high-speed capabilities of its advanced fiber Bragg grating (FBG) sensing and optoelectronic interrogation technology to enable real-time high-speed measurements of dynamic strain, shock, and vibration signals as well as their wideband spectral signatures as indicators of rail integrity (health) condition, both reliably and autonomously, while the train is in motion.

Innovative IFOS Approach to Broken Rail Detection

The IFOS RailSense™ system is a cost-effective, multipoint, multifunction fiber-optic sensor system for broken rail and defect detection. Laboratory demonstrated in this program, it has the potential to provide rail breakage detection capability with high resolution (~1 mm at 65 mph train speed), and high accuracy at high monitoring speeds (~1 Mega-samples per second or ~1 MS/s, per sensor). RailSense provides the ability to detect rail breakage where inspection tools such as NDT, hand-held inspection, visual inspection, and signaling are either unavailable or impractical.

Figure 2 shows details of the FBG sensor array installation on a freight car wheel-axle-boxes. The design involves tri-axial set of FBG sensors installed on each of the left and

right axle boxes. Signals from the FBG sensor arrays are sampled at up to 1 MS/s with 16-bit resolution. Recorded data is processed for rail breakage identification.

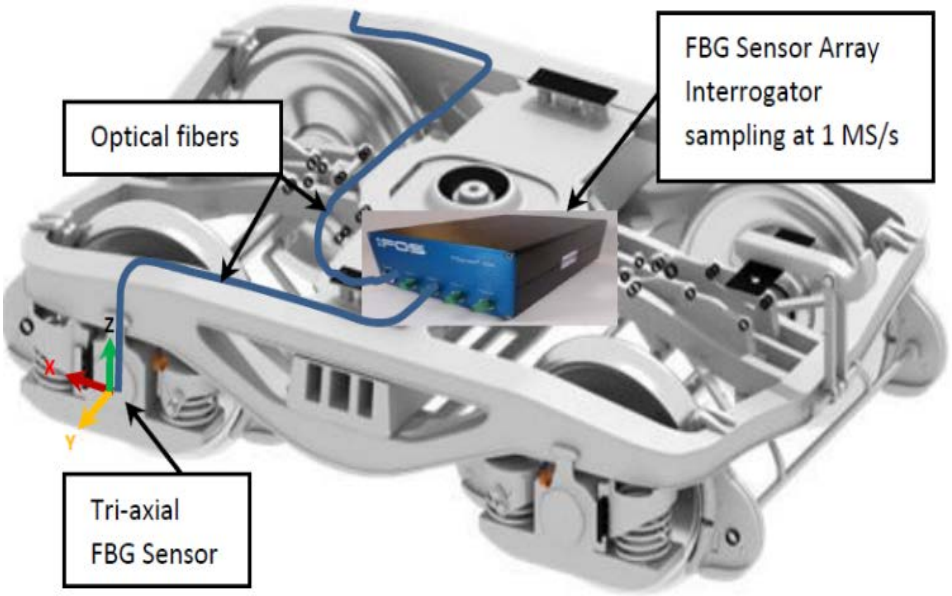

Figure 2: FBG sensor array installation on the freight car wheel-axle boxes [12].

Investigation

Our investigation involved computer simulation, lab tests and algorithm development. In the following subsections, the team discusses a test rig simulation of a train passing over localized rail breakage including a wheel passing over broken rail simulated by a hammer impact. Then the team provides experimental results and an algorithmic approach to the analysis of those results including simulation of the effect of environmental noise and wheel flats. The latter approach involves wavelets (described on p.17) as a measure of the intensity of the broken rail signal,

Test Rig Simulation

An 8" diameter wheel has been used to simulate the event of a heavy revenue train passing over a rail with localized breakage. Since the weight to stiffness ratio of the lab set up is much smaller than that of the actual train, the dynamic response that has been measured using the FO sensor system contains much lower amplitudes than those measured on a real full-scale track. Although this may be of concern, in this feasibility study, the idea has been to test the algorithm with the sensor data to check both the integrity of the sensing data and the viability of the algorithm to detect the breaks/defects (corrugations) even when the acceleration/strain data values have much lower amplitudes than those collected on an actual train (involving because of the higher train weight and larger wheel diameter).

To show this, V3T developed a computer model of the train-wheel-track system to simulate the acceleration signals induced in wheel of a trolley of 1000 lbs moving on a broken rail at speeds of few meters per seconds. Figure 3 shows the simulation results. The results show very distinctive acceleration signals (with relatively low amplitudes) when the wheel hits the 5 mm wide break. The highest simulated acceleration level is approximately 10 g (g = 9.8 m/s^2) over a time interval of approximately 10 ms.

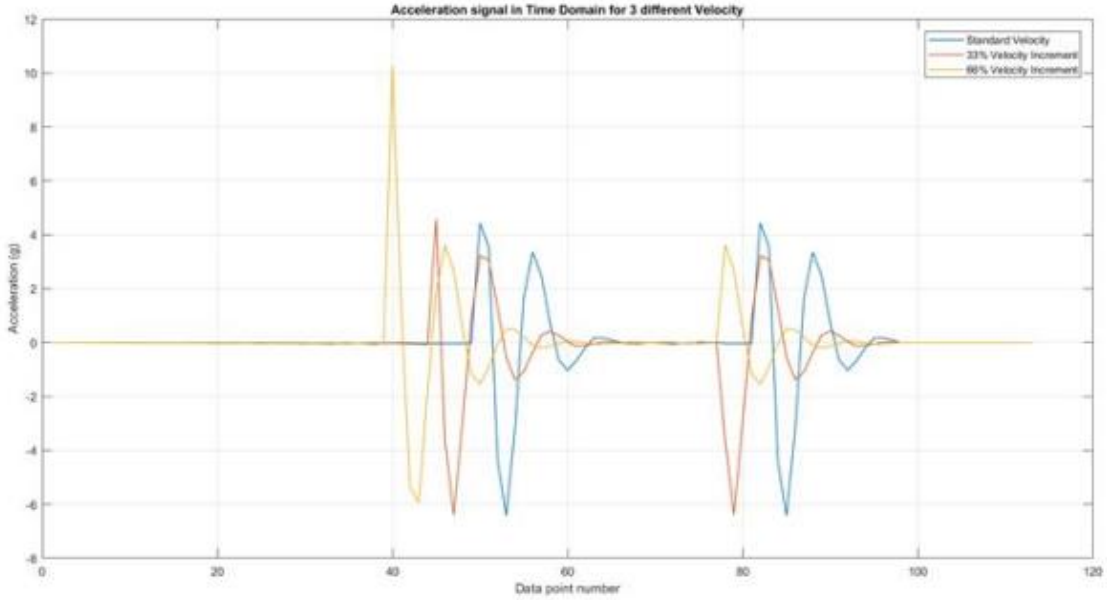

Figure 3: Acceleration induced in wheel of a trolley of 1000 lbs moving on a broken rail.

In next section the team describes the lab test setup used to produce series of transient acceleration pulses (as shown in Figure 3) in an 8" diameter wheel. The purpose of this experiment is to demonstrate the capability of the FO sensing system in detecting the simulated event of the wheel hitting a breakage point in the rail in real time.

Wheel-Broken Rail Simulation – Hammer Impact Test Setup

IFOS has constructed and assembled an experimental setup to simulate an 8" scaled train wheel in motion that receives a 10 g acceleration over 10 ms mechanical shock. The wheel used in the experiment is a single flanged track wheel with an 8" diameter, 2-1/4" face, 3-1/4" hub length, and 1" roller bearing from Service Caster (SCC-WFT-82H-1). A 1" diameter, 30" long axle is used to mount the wheel. Two clamps are used to keep the wheel at the center of the axle. The weight of the wheel with the axle and the hanging chain is 35 lbs. A digital inclinometer (Meterk E3702) is attached to the side surface of a sledge-hammer head to measure the pendulum angle of the hammer. The weight of the hammer with the hanging chain is 14 lbs. The distance between the hanging point to the weight center of the wheel is 47.8", and 47.5" to the hammer head.

As shown in Figure 4 an accelerometer (model MEAS 4000A-010) has been mounted on the 8" scaled train wheel behind the hammer impact location to monitor the level and duration of the shock induced in the wheel during the impact event. An oscilloscope is used to measure the output of the accelerometer.

In order to induce a mechanical shock in the 8" scaled wheel with a peak acceleration of 10 g and a duration of 10 ms, damping materials with various lift angles of the hammer have been tested. The optimal impact damping material has been found to be a white foam pad with a thickness of 1/2" attached to the wheel, combined with a clear rubber feet bumper pad (12.7x3.5mm cylindrical shape) attached to the center of the hammer impact surface. The optimal lift angle of the hammer has been found to be 24°.

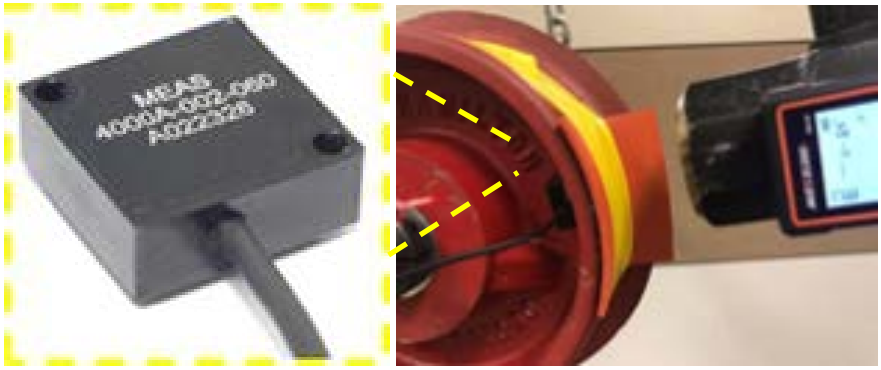

Figure 4: Accelerometer (model MEAS 4000A-010) mounted on the 8" scaled train wheel.

As shown in Figure 5, an array of three FBGs labeled as Sensors 1, 2 and 3 have been attached to the wheel axle, which is a solid steel bar. The acrylate coating layers of the optical fiber over the three FBGs are removed prior to attaching the sensors to the wheel axle using instant adhesive (Weld CA40). This allows for maximum dynamic strain

coupling to the FBG sensors. Sensor 1 has been mounted in the longitudinal direction for measuring strain in the horizontal direction. Sensors 2 and 3 have been attached orthogonally with respect to Sensor 1 for the purpose of Sensor 2 measuring vertical strains and sensor 3 measuring horizontal strains, perpendicular to Sensor 1. The distance from the wheel side surface to Sensors 1, 2, and 3 are 188 mm, 103 mm, and 123 mm, respectively.

Responses of the three FBG sensors, during the hammer impact tests, have been recorded using IFOS' high-speed interrogator (shown in Figure 6) at a sampling rate of 500 kilosamples per second (500 kS/s). Strain values have been calculated from the FBG center wavelength shifts.

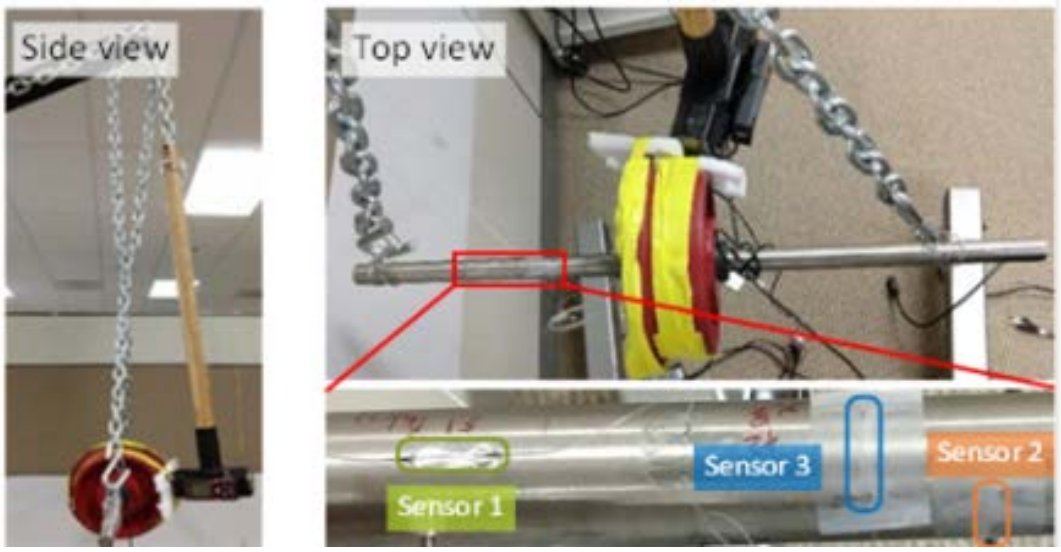

Figure 5: Experimental setup for hammer impact measurements with FBGs and an IFOS high-speed interrogator.

Figure 6: IFOS' High-Speed FBG Interrogator

Experimental Results

This section describes the experimental results of the aforementioned hammer tests. During these tests, the accelerometer response has been recorded using an oscilloscope in single trigger mode. The red curve in Figure 7 shows one of such acceleration time histories with the peak of acceleration at around 10 g (corresponding to 98 m/s^2 acceleration), with a pulse width of around 10 ms. The strain response of Sensor 2 with inverted amplitude is also shown as the black curve in Figure 7. The maximum dynamic strain measured by Sensor 2 is around 35 με.

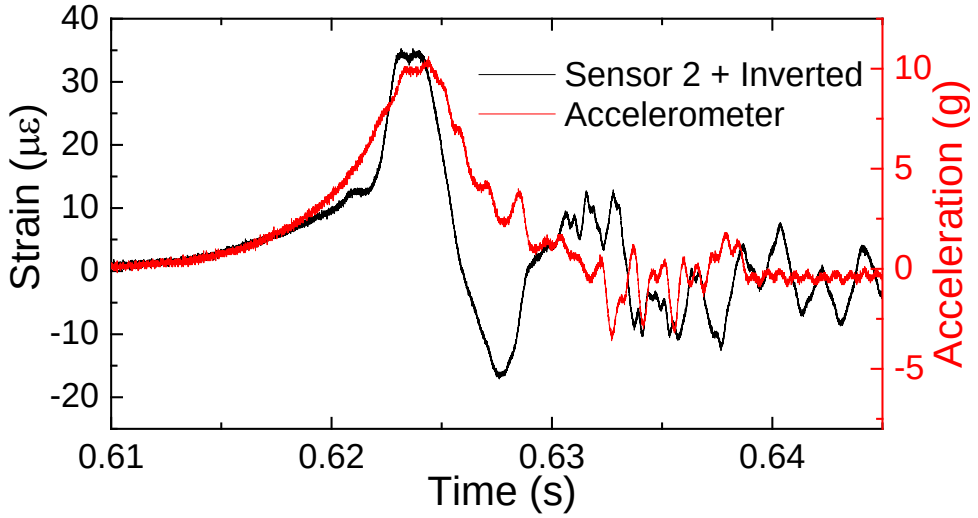

Figure 7: Responses to the hammer impact.
Red: Accelerometer; Black: FBG sensor 2 with inverted amplitude.

Two seconds of strain time histories associated with the three FBG sensors are shown in Figure 8. The first impact around 0.6 seconds is zoomed in and shown on the top of Figure 8, and second impact around 1.4 seconds caused by the hammer second hit is zoomed in and shown at the bottom of Figure 8. It is worth noticing that Sensor 1 and Sensor 3 have completely opposite responses to both impacts, while sensor 1 has a larger magnitude than Sensor 3.

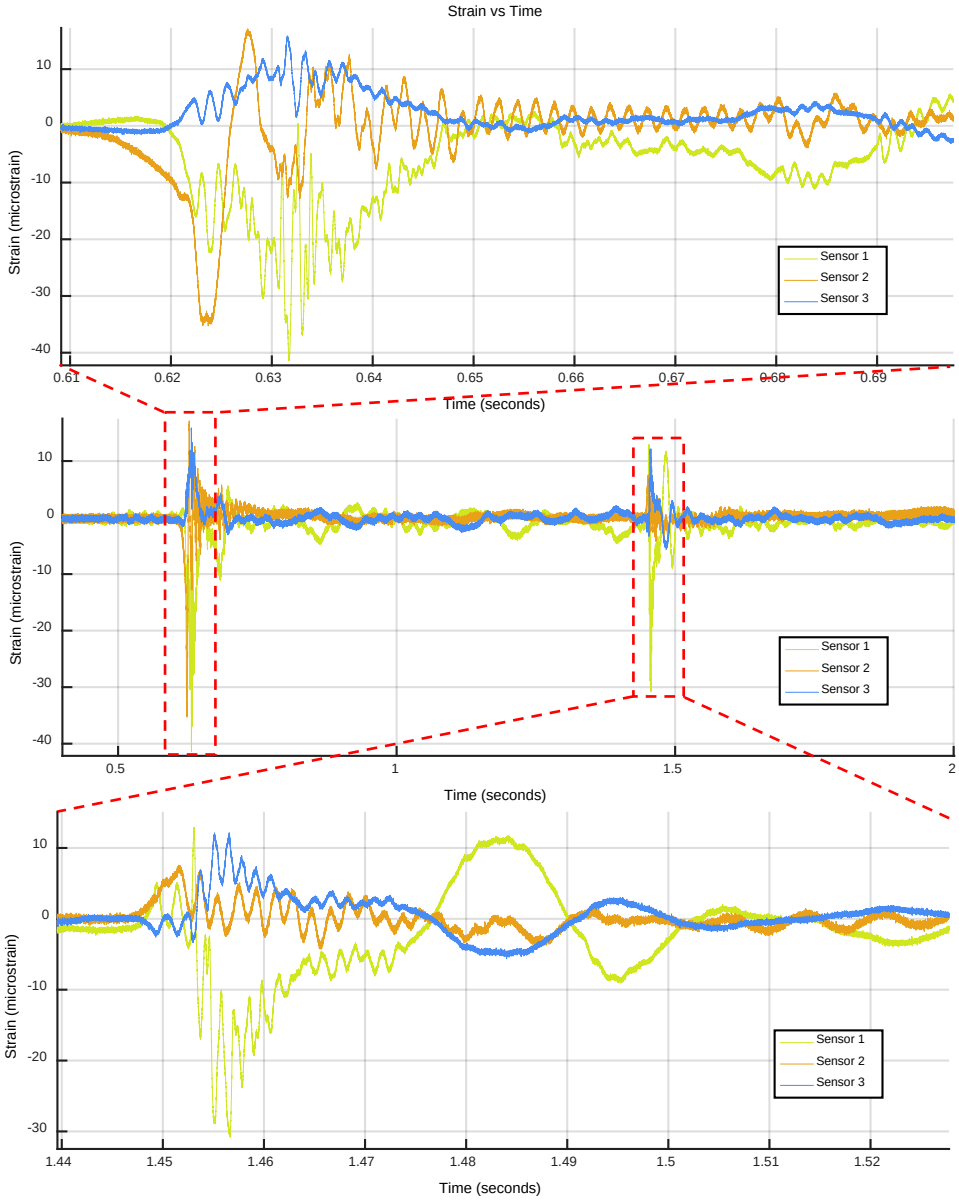

Figure 8: Strain changes of the FBGs. Top: First impact around 0.6 seconds; Bottom: Second impact around 1.4 seconds.

Theory of Wavelet Analysis and Intensity Factor

A wavelet is a wave-like oscillation with an amplitude that begins at zero, increases, and then decreases back to zero. Wavelets provide a good representation of a pulse of wave energy and, as the team demonstrated in [12], are suitable for analyzing events related to broken rail [4, 12]. Mallat [13] showed that the local regularity of a signal can be estimated by using the wavelet transform to calculate the Lipschitz exponent at each time step in the signal. The developed formulas can be used to gain insight into the power of the wavelet transform in locating irregularities in a signal. This method can also be used to calculate the Lipschitz exponent directly to provide information that can be used in event detection and classification. The premise is that the decay of wavelet coefficients across wavelet transform scales can be related to the value of the Lipschitz exponent. Since the wavelet transform provides localization in the time domain, the time local Lipschitz exponent can be estimated.

Mallat showed that the regularity of a function at any point $t = t_0$ can be estimated by observing the decay of the wavelet coefficients of the continuous wavelet transform (CWT) across scales, s. It was shown that a function $f(t)$ is uniformly Lipschitz α if and only if there exists some non-negative constant A such that:

$$|Wf(s,u)| \leq As^{\alpha}$$

where $Wf(s, u)$ are the wavelet coefficients calculated from:

$$Wf(s,u) = \frac{1}{\sqrt{s}} \int_{-\infty}^{+\infty} f(t)\psi^*\left(\frac{t-u}{s}\right) dt$$

Taking the logarithm of both sides of the above Equation gives:

$$\log|Wf(s,u)| \leq \log(A) + \alpha \log(s)$$

The modulus maxima of the wavelet coefficients can then be plotted as the ordinate with scale s as the abscissa with log scale for each location u. The Lipschitz exponent α can then be determined for each location on the time axis by fitting the data to the above equation with a linear least-squares regression. The Lipschitz exponent describes the type of singularity, or in other words, the degree of regularity. Therefore, the sharper the irregularity, the lower the value of the Lipschitz exponent. It has been shown that the severity of the defect can be calculated by the value of A, which is referred to as the intensity factor (*IF*).

To establish grounds for the intensity factor, A, a CWT was applied to the fundamental vibration mode of a cantilever beam both analytically and experimentally. The above equation was used to calculate both the values of the Lipschitz exponent, α, at regular spaced intervals across the beam and the depth of the crack by relating it to the intensity factor A. Since singularities of the same type are characterized by the same α value, it was expected that all cracks of the same type would have the same α value. Therefore, for a fixed crack type and fixed α, the intensity factor A is the only variable that changes in the above equation. Intensity factor was therefore related to crack severity or depth.

Rail Break Detection by Wavelet Analysis

V3T applied digital signal processing for rail break detection techniques using the experimental data by calculating the intensity factor (*IF*), a measure of the intensity of the signal, calculated by a wavelet algorithm. Wavelets, introduced in the previous subsection, are defined using scaling factor, scaling function, or wavelet function. Wavelets can be used to extract information from various types of data. Multiple sets of wavelets are usually required to fully analyze data. Figure 9 shows the preliminary results indicating the successful identification of simulated rail breakage events.

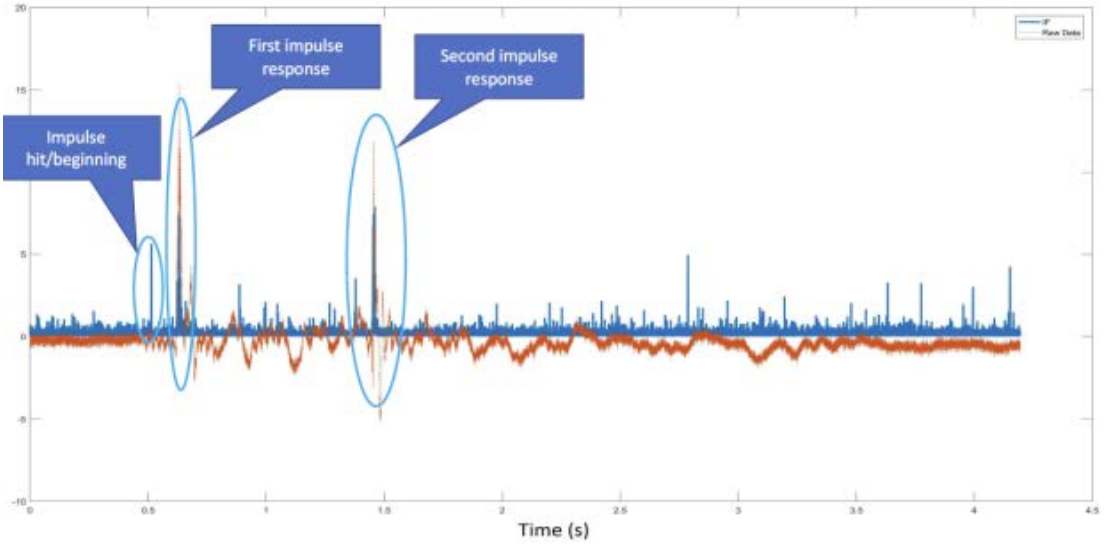

Figure 9: Preliminary Analysis of Experimental Data Showing Intensity Factor (IF) calculated by Wavelet Analysis.

Rail Break Detection by Wavelet Analysis with Environmental Noise

In order to assure robustness of the defect detection algorithm to noise, acceleration data previously collected at 9600 Hz was de-noised and the noise data from this signal was resampled to match the sampling rate of the data collected during the Stage I testing. To be representative of typical noise present in the field, the acceleration time history from which the noise signal was extracted, was collected on a rail track during one of the Association of American Railroads (AAR) tests using a real-time computer (Speedgoat) and a tri-axial accelerometer attached to the train wheel axle. This noise data was then added to the experimental hammer test data collected using the IFOS FBG-based sensing system. The new data with filed-representative added noise was then processed, the intensity factor calculated and compared to the original noise-free data.

Figure 10 shows the comparison between the two results. As can be seen, the added field-representative AAR-collected environmental noise has no negative impact on the identification of the rail break condition. Additionally, the spike in the *IF* at 0.5 seconds, which had a larger value for the data without noise (in orange) has a smaller magnitude for the data with noise (in yellow). This is due to the fact that the original data itself contains noise. Adding noise to signals, especially well designed pink noise (only

coincidence in this case), is a technique that has been used to improve feature extraction from signals [14].

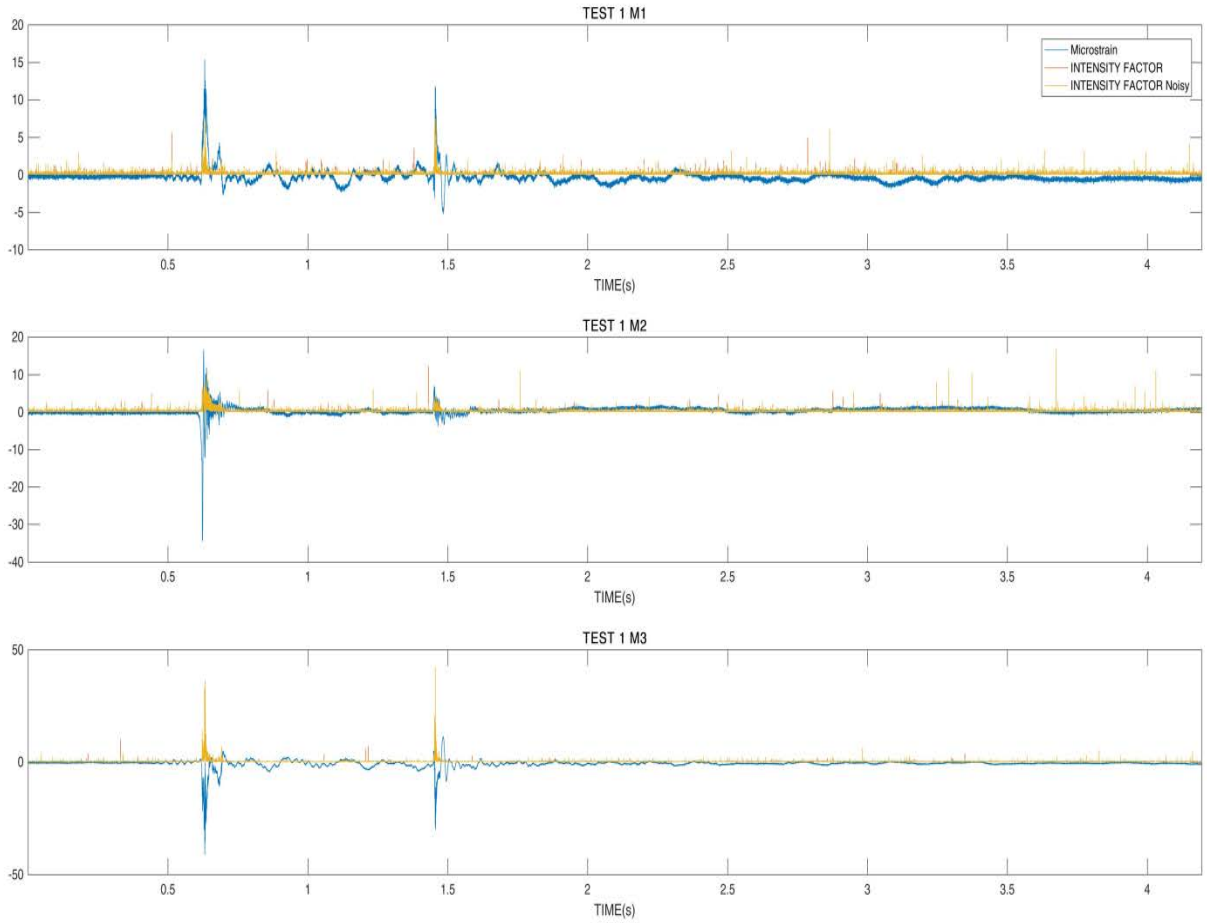

Figure 10: Intensity Factor results with and without noise

Computer Simulation of Wheel Flats

The team developed a MATLAB program to simulate effects of train wheel flats on the wheel axle. The purpose of this exercise was to add the simulated signals as noise to the existing hammer test data, for further processing by the wavelet analysis and to demonstrate the capability of differentiation between the wheel flats and rail break events.

The first step is to produce a transient similar to the graph shown in Figure 11 from Liang-2013 [9].

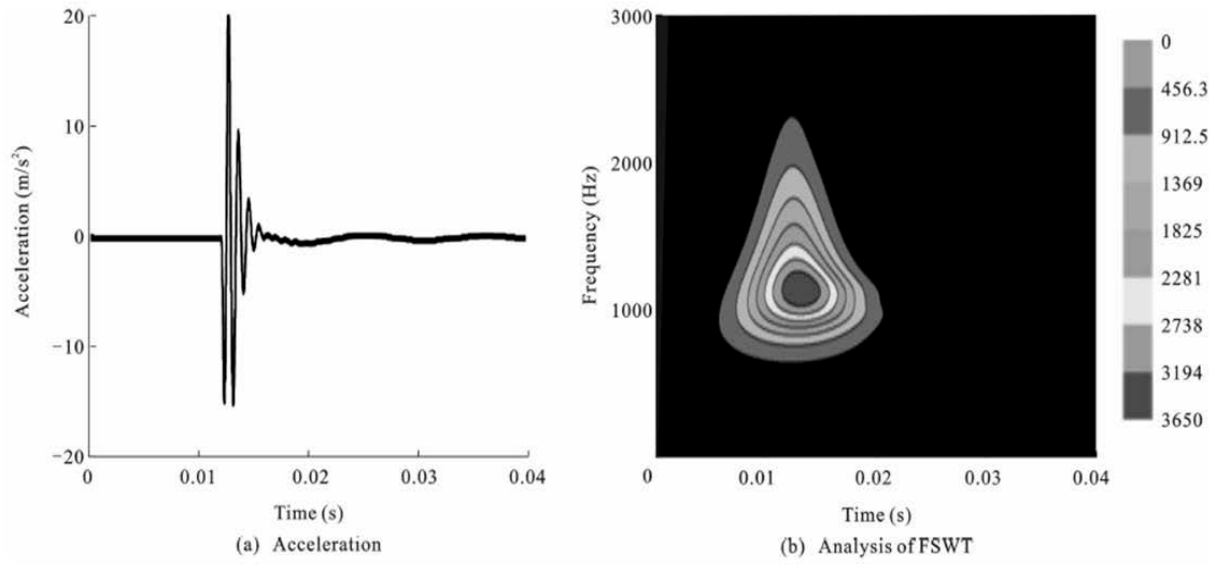

Figure 11: Time history of acceleration and its time-frequency analysis (train velocity 50 km/h, wheel flat length = 10 mm)

For consistency, the y-axis units in Figure 11-a should be converted from m/s^2 to microstrain. The following paragraph describes the scaling process.

Based on the simulations performed earlier in the TRB project, acceleration induced in the wheel of a trolley of 1000 lbs moving on a broken rail at speeds of few meters per seconds hitting a 5 mm wide break in rail is approximately 10 g (g = 9.8 m/s^2) over a time interval of approximately 10 ms. Hammer tests, on a scaled 8" wheel showed that a 10 g - 10 ms impact on the wheel produced the following peak strain values on the wheel axle (See Figure 8):

Sensor 1: 40 microstrain
Sensor 2: 35 microstrain
Sensor 3: 15 microstrain

Therefore, the team could use a scaling factor of peak microstrain/10 g to scale the amplitude (converted to g) of the transient pulse shown in Figure 11-a to find the amplitude of the simulated waveform in terms of microstrain. The calculated scaling factors are as follows:

Sensor 1: 40/10 = 4
Sensor 2: 35/10 = 3.5
Sensor 3: 15/10 = 1.5

The x-axis scaling is the same as the one shown in the plot.

Figure 12 shows the simulated (single pulse) wheel flat signal for the three sensors.

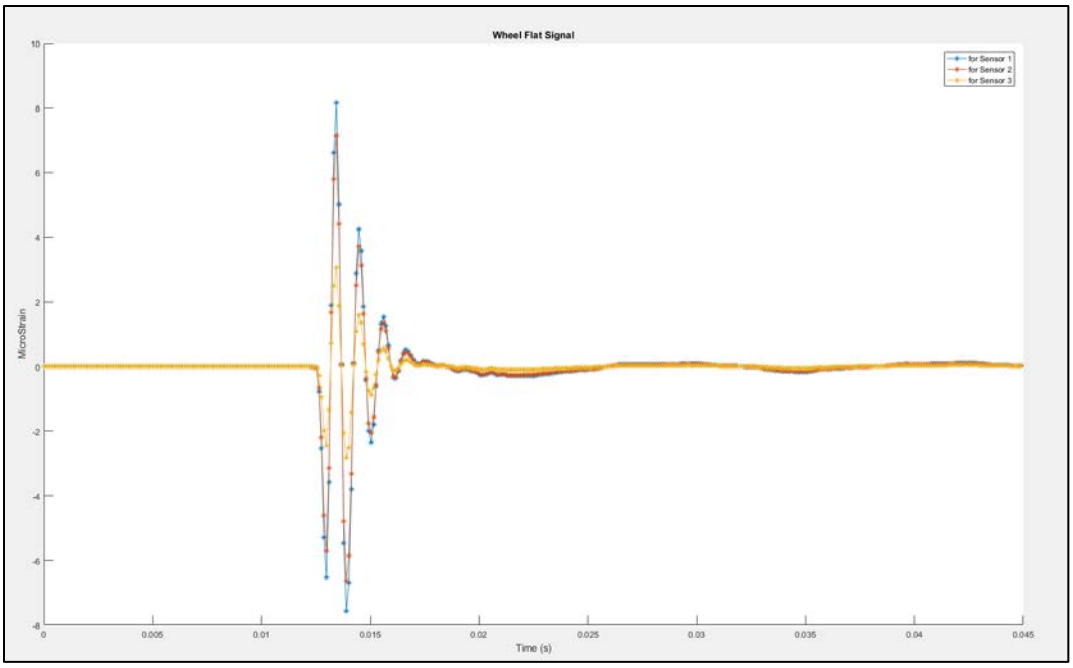

Figure 12: Simulated wheel flat signal for at FBG sensor locations 1, 2 and 3

Since wheel flats apply a periodic force on the wheel axle as the wheel rotates, a periodic time history should be created by repeating the simulated signal as described above. *T*, the periodicity of the wheel flat force, is set by the wheel size and the train speed as follows:

$T = \pi * D/v$ where *T* is the wheel-flat force period, *D* is the wheel diameter and v is the train velocity. Given the scaled wheel diameter of 8" for a train speed of 50 km/h (from the plot above) *T* can be calculated as 45 milliseconds (ms).

The last step is adding the simulated wheel-flat periodic signals to the corresponding strain data previously recorded during the hammer tests.

Wavelet and Intensity Factor Analysis of Hammer Test Data with Simulated Wheel Flat Data Added

In Figure 13, the window on the top-left corner shows the raw-data, on which this short analysis was performed. In blue, the measurement signal is plotted, while the dotted orange line represents the measurement plus the flat-wheel simulation. The blue line is not clearly visible because it is almost entirely covered by the orange line. On the time scale, slightly after 2 seconds, the flat-wheel data ends, and the team can see that the orange and the blue lines are identical.

In the time-range 0-2 seconds, the orange line deviates clearly from the blue line whenever there is an oscillation. These oscillations are due to the flat-wheel responses. To show better the difference between the measurement signal and the measurement

with flat-wheel data, an enlargement box of the time-range 0.5-1 seconds is shown on the right-bottom corner.

The right-bottom corner shows that the orange line oscillates periodically, but the blue line does not follow it; the dotted line is not accompanied by the blue in these oscillations. The light-blue shaded oval area highlights the amplitudes of the flat-wheel data with respect to the *X*, *Y* and *Z* measurements of the rail (assuming the same signal unit for both the measurement and the flat-wheel data). If the flat-wheel signal is considered a noise, the team can see that the Signal-to-Noise-Ratio (SNR) is the largest with the *Z* measurement (Sensor 3, the bottom plot), while it is the smallest with the X measurement (Sensor 1, the top plot). This observation makes the *Z* (Sensor 3) the best candidate signal to use for primary analysis and distinguish the rail break signature from the flat-wheel signature.

The intensity factor computation is a wavelet-based identification algorithm that computes the Lipschitz Exponent of signals. It detects sharp changes and irregularities in signals.

Figure 14 shows the results of computing the *IF* of the signals in Figure 13. These plots show the results of running the data through the *IF* algorithm. The figure plots the data analyzed (blue) on top of the intensity factor results for the rail measurement (orange) and the rail measurement with flat-wheel data (yellow). The window on the top-left corner shows that the IF algorithm is consistent in identifying the irregularities in the signal. Both the two breaks and the flat-wheel oscillations are identified.

The window on the right-bottom corner shows a zoom on a couple of the flat-wheel oscillations, and the three signals are better identified.

It is difficult from processing the measurements of Sensors 1 and 2 to identify the breaks if the measurement includes flat-wheel responses. However, the *Z* measurement (Sensor 3, bottom plot in Figure 14) shows that the *IF* values of the breaks are well-distinguishable from the flat-wheel oscillations. The breaks give *IF* values larger than 30, while the flat-wheel oscillations yielded *IF*s smaller than 20.

These are considered preliminary results. Many techniques can be used to improve the quality of identification, changing the mother-wavelet of analysis showed very good preliminary results. This explains post processing of the data. However, the real-time version of the algorithm gives similar results, where the irregularity can be identified with a very short time-delay, less than or of the order of milliseconds, from the moment the irregularity is sensed.

The time-delay depends on the power of the computer/microprocessor performing the computations. Moreover, filtration techniques, classical and non-classical, are additional ad-hoc processors to ignore or completely filter-out the flat-wheel signature if needed.

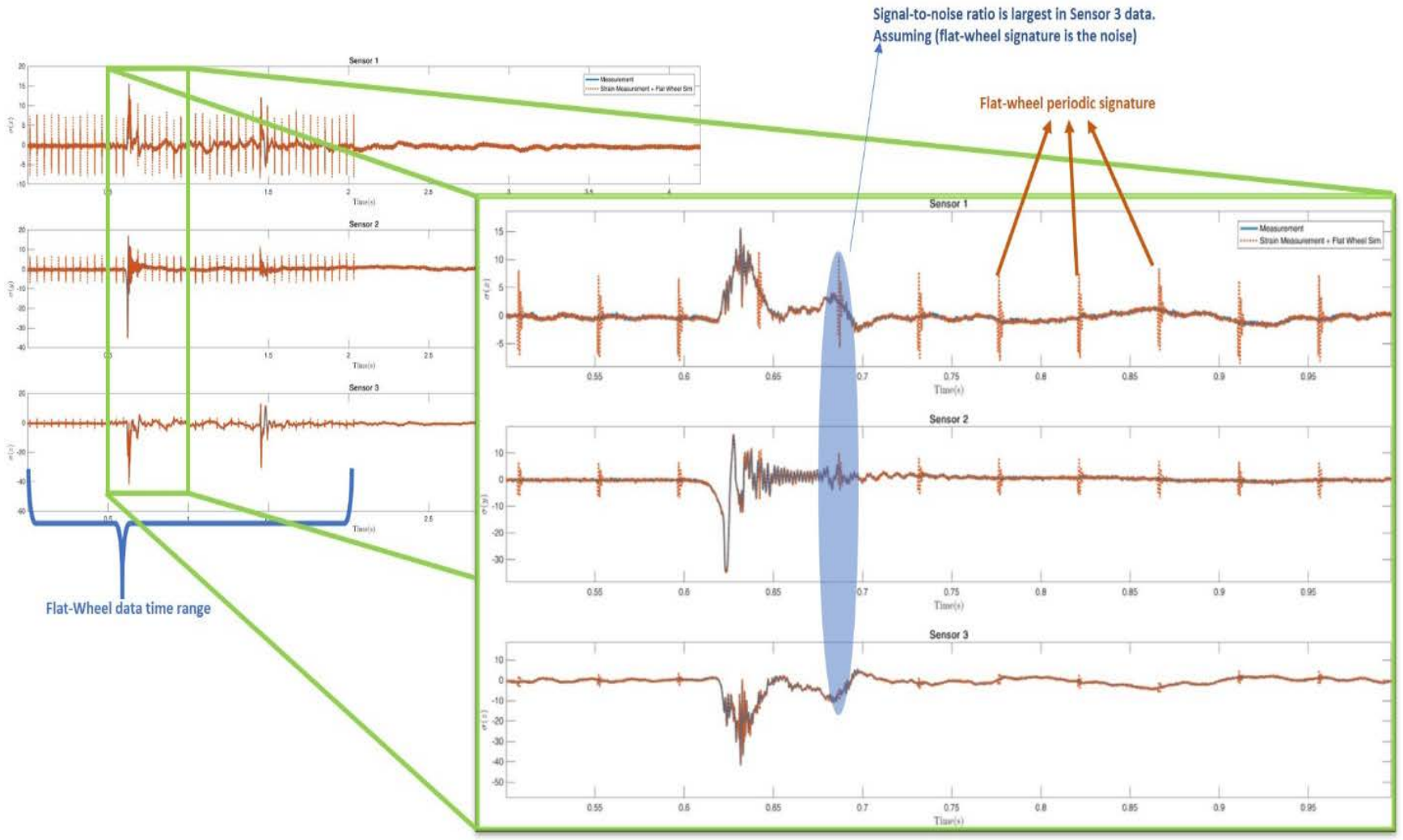

Figure 13: Hammer test measurements with added flat wheel simulated signals

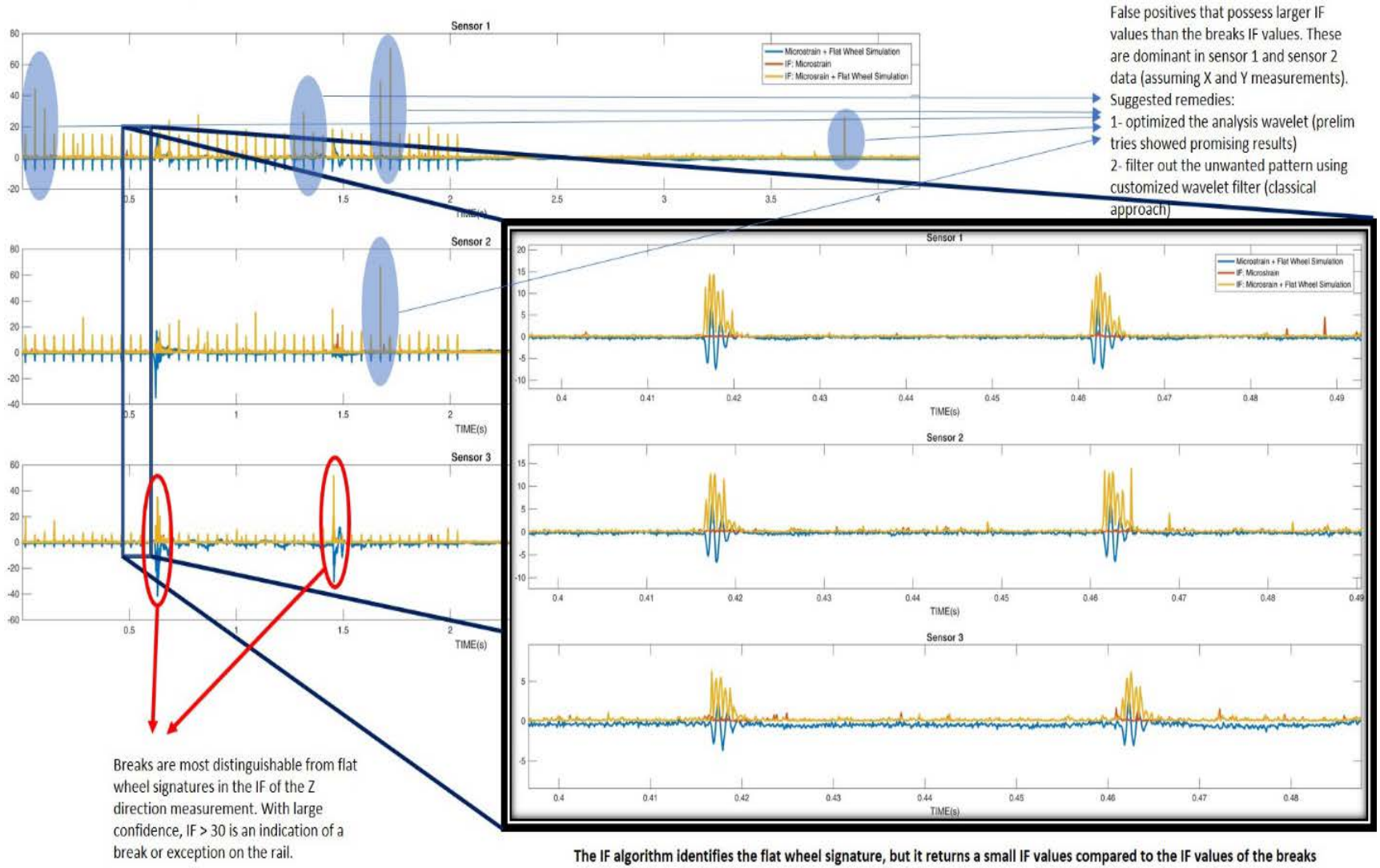

Figure 14: Intensity Factor results of hammer test measurements with added flat wheel simulated signals

Plans for Implementation

IFOS' proposed onboard FO sensing system provides the ability to detect rail breakage where inspection tools such as non-destructive testing (NDT), handheld, visual inspection or signaling are either unavailable or impractical.

Collecting data in the field is a crucial next step. IFOS plans to conduct testing in a relevant environment in collaboration with a leading U.S. transportation testing facility to pave the way for commercialization.

In follow-on work, as opportunities arise, as well as pursue implementation of the on-train broken rail detection technology developed in this program, the team plans to examine both on-track and on-train sensing signatures for wheel flat signatures. Work to date indicates that this approach avoids false positives. This will be critical to confrm in the field. IFOS' rail break detection system can be used to collect data on characteristics of rail breaks including their size, locations and numbers. Collected data analytics can be used to enhance the general maintenance procedures.

Differentiating rail conditions: In addition to broken rail and wheel flat detection, the proposed approach has potential for differentiating various conditions including rail separations (broken) from shelled areas or wheel burns (from spinning) or joints. With regards to joints versus breaks

- The gap between the two rails in a joint ranges from 0" when the rails are hot, to about 0.56" [15] when the rails are cold. For a broken rail, there is a gap between 0 and 12-16 inches; usually 1-4 inches [16].
- When the break is over 0.56", the difference in the gaps in the rail associated with a joint vs a break translates into an identifiable difference in the signatures of measured signals (pulses) especially when measured at high sampling rate by the IFOS' onboard interrogator.
- When the break is in the range 0-0.56" (typical range for a joint, and the type of break that a track circuit cannot detect [16]), known rail joint positions combined with the train GPS data can also be used to differentiate between broken rail and joints in the rail. As pointed out by an anonymous reviewer, distinguishing rail joints and surface defects from actual broken rails, may also be facilitated by comparing accelerations from run to run. The ability to precisely locate the various signals manifest in the IFOS system then becomes particularly important.

The above is an area where the team plans further validation work as the opportunity arises.

Preliminary Spinoff Commercial Application: To complement the laboratory (simulated on-train) testing in this project, IFOS also performed some sensor-on-track testing using its I*Sense FBG interrogator and under-rail FBG sensors to both register passing train sizes (axle count) with the potential to consider the health of rolling stock. The following figures show some example results. In particular, Figure 15 shows the response to train passage of five underail fiber optic sensors on a fiber attached to an IFOS I*Sense 48K interrogator. We note the signature of the engine (heavy) and medium and light wagons – see also [17]. Figure 16 shows a zoom of the initial part of the Figure 15. Figure 17 shows measurement of decelerating, stopping then accelerating resulting

in an accordion-like strain signature. These figures, particularly Figure 16, show [18], as expected, the wave of compressive strain before and after the train wheel passes the sensor, and the larger tensile strain when the train wheel is above the sensor. The inset exagerates this effect to illlustrate the concept – Even the heavy (locomotive) leads to a maximum under-rail tensile strain (fractional elongation) of less than 1000 microstrain (ppm) or 0.1%.

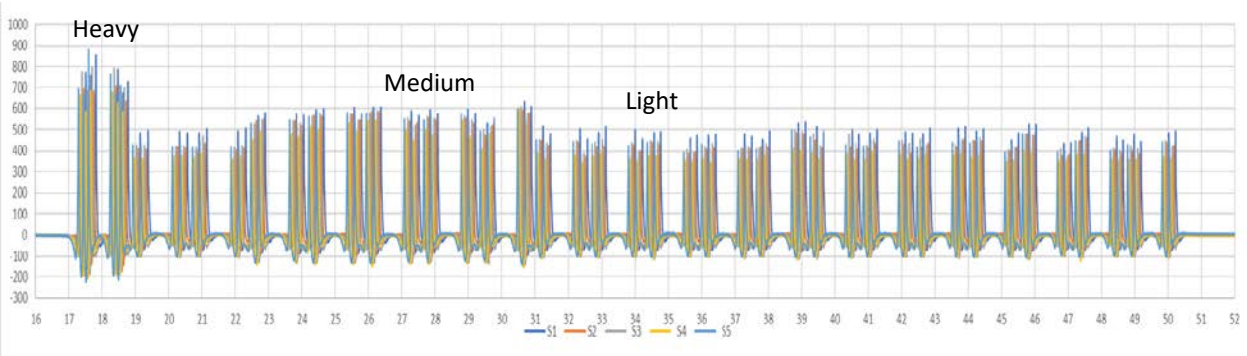

Figure 15: IFOS I*Sense® interrogator measurement of passing train. Traces for 5 sensors are shown.

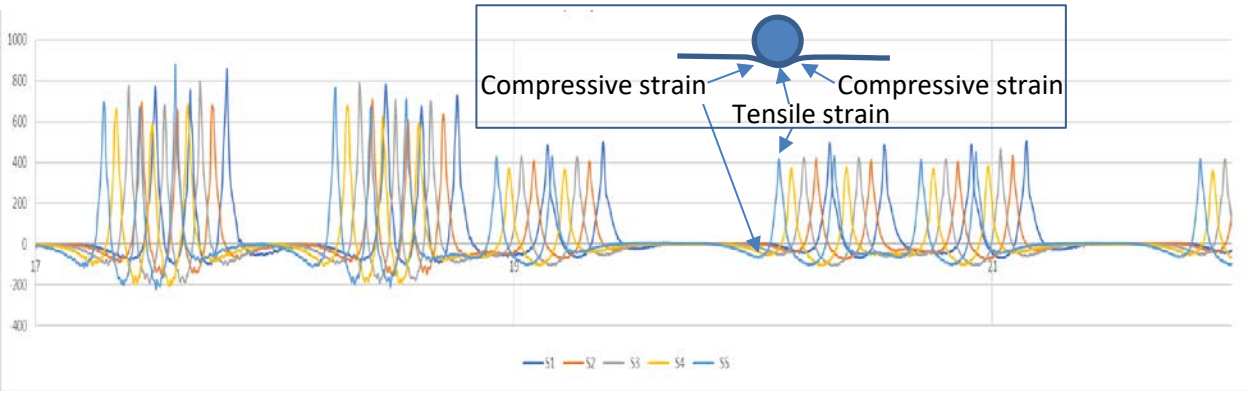

Figure 16: Zoom of initial part of previous figure.

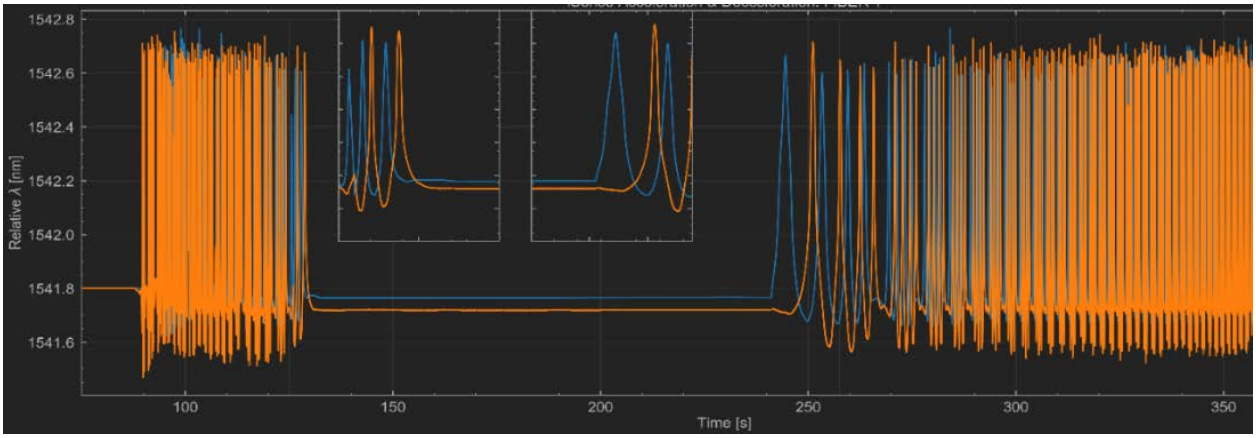

Figure 17: IFOS I*Sense interrogator measurement of decelerating, stopping then accelerating train for 2 sensors. (Wavelength change of 1.2 nm corresponds to 1000 microstrain.)

Conclusions

A variety of methods have been employed to improve the reliability and the timeliness of detecting rail breaks on railway lines throughout the world. Typically, these methods are applied at scheduled times, resulting in extended periods during which rail breaks are not detected. These methods are manpower intensive, expensive to execute and sometimes interfere with train operations. Rail breaks are a serious threat to rail especially when large day to night temperature swings are encountered. While inspections, using conventional ultrasonic and magnetic induction techniques, are performed periodically and repairs are made when cracks are detected, rail breaks are still a significant occurrence around the world [19]. Fortunately, only a fraction of these results in train derailments [20].

IFOS RailSense™, using a high-speed fiber-optic sensor interrogation [21, 22], has been designed to enable autonomous measurement of strain, shock, and vibration signals as indicators of rail and train condition while the train is in motion. During this project, the IFOS R&D and engineering team used computer simulations of the train-wheel-track system and designed a test in the lab for simulating the event of the train wheel hitting a breakage point in the rail. The team developed signal processing algorithms for detection of the rail break signals in presence of noise. Environmental noise as well as wheel-flat transients were added to the lab test data and we demonstrated that the signal processing algorithms perform well in presence of noise and spurious signals.

What makes these results meaningful to the railway industry is that they provide confidence that false positives can be avoided and when such a system is deployed for regular rail usage it would have the potential for early detection of rail breaks and wheel flats and thus significantly reducing the possibility of derailment. The IFOS system may have the potential to replace or complement current sensors with augmented performance. In addition, IFOS fiber optic sensors systems can provide multi-functional temperature, quasi-stratic strain (loading) and vibration measurements as well all using a single interrogation system. Such technology has significant potential for instrumented wheel sets.

- While track circuits already do a reasonably effective job detecting broken rails in signaled territory, the system can augment existing track circuit-based broken rail detection by identifying partial breaks and breaks that span a conductive medium such as a tie plate, and also identify the precise location of the break, which track circuits do not.
- In non-signaled (dark) territory, the system using vehicle-mounted sensors can act as the primary broken rail detection methodology, far exceeding the performance of the existing methodology of visual inspection.
- In response to those who comment that if one cannot find the rail break until the locomotive is on top of it, it is too late, we note that rail breaks occur most often under a train due to dynamic interaction of wheel forces with weak locations on the rail. For optimal protection, it is recommended the system be installed on a data processing unit (DPU) on the rear of the train, so that any breakage that occurs during that train's passage over a section of track

can be detected and sent as an alert before the next train arrives. Train make-up thus becomes a key to the effectiveness of this system.

To conclude [18], the FBG sensors provide the top combination of high-speed and ultra-low noise and high dynamic range measurements in a single package. This report successfully illustrates how this technology can be used to perform real-time signal processing to extract the smallest details to be able to differentiate between track breaks and common surface defects.

Such a system would be particularly useful if deployed in a way that it repeatedly captured and compared changes the rail signature over time. It could even be more effective than the current signaling system if combined with the ability to measure/monitor rail strain (e.g., using photoluminescence or piezospectroscopy). It would also be a superior wheel counting and wheel assessment technology when applied as shown in the spinoff application (p. 23), provided that it is cost competitive, which we expect it to be.

References

[1] D. F. Thurston, "Broken rail detection: Practical application of new technology or risk mitigation approaches," *IEEE Vehicular Technology Magazine*, vol. 9, no. 3, pp. 80-85, 2014.

[2] S. Mariani, T. Nguyen, X. Zhu, and F. Lanza di Scalea, "Field test performance of noncontact ultrasonic rail inspection system," *J. Transport. Eng., Part A*, vol. 143, no. 5, p. 04017007, 2017.

[3] F. A. Burger, "A practical continuous operating rail break detection system using guided waves," in *18th World Conference on Nondestructive Testing*, 2012.

[4] B. M. Hopkins and S. Taheri, "Broken rail prediction and detection using wavelets and artificial neural networks," in *ASME/IEEE Joint Rail Conference*, 2011, vol. 54594, pp. 77-84.

[5] W.-J. Cao, S. Zhang, N. J. Bertola, I. F. Smith, and C. G. Koh, "Time series data interpretation for 'wheel-flat'identification including uncertainties," *Structural Health Monitoring*, p. 1475921719887117, 2019.

[6] R. Gao, Q. He, and Q. Feng, "Railway wheel flat detection system based on a parallelogram mechanism," *Sensors*, vol. 19, no. 16, p. 3614, 2019.

[7] R. Gao, Q. He, Q. Feng, and J. Cui, "In-Service Detection and Quantification of Railway Wheel Flat by the Reflective Optical Position Sensor," *Sensors*, vol. 20, no. 17, p. 4969, 2020.

[8] L. Han, L. Jing, and K. Liu, "A dynamic simulation of the wheel–rail impact caused by a wheel flat using a 3-D rolling contact model," *J. Mod. Transportation*, vol. 25, no. 2, pp. 124-31, 2017.

[9] B. Liang, S. Iwnicki, G. Feng, A. Ball, V. T. Tran, and R. Cattley, "Railway wheel flat and rail surface defect detection by time-frequency analysis," *Chem. Eng. Trans.*, vol. 33, 2013.

[10] T. Snyder, D. Stone, and J. Kristan, "Wheel flat and out-of round formation and growth," in *Proceedings of the 2003 IEEE/ASME Joint Railroad Conf.*, 2003: IEEE, pp. 143-148.

[11] S. Kumar, *Study of rail breaks: associated risks and maintenance strategies*. Luleå tekniska universitet, 2006.

[12] S. Taheri, B. Moslehi, V. Sotoudeh, and B. M. Hopkins, "Rail Defect Detection Using Fiber Optic Sensors and Wavelet Algorithms," in *ASME/IEEE Joint Rail Conference*, 2018, vol. 50978: American Society of Mechanical Engineers, p. V001T10A002.

[13] S. Mallat and W. L. Hwang, "Singularity detection and processing with wavelets," *IEEE transactions on information theory*, vol. 38, no. 2, pp. 617-643, 1992.

[14] M. D. Skowronski and J. G. Harris, "Improving the filter bank of a classic speech feature extraction algorithm," in *Proceedings of the 2003 International Symposium on Circuits and Systems, 2003. ISCAS'03.*, 2003, vol. 4: IEEE, pp. IV-IV.

[15] Constantin. "Maximum joint expansion gap." https://pwayblog.com/2016/03/04/maximum-joint-expansion-gap/ (accessed 11/28/20, 2020).

[16] T. Bartlett, "Personal Communication," ed, 2020.

[17] H.-Y. Tam, S. Liu, S. L. Ho, and T. K. Ho, "Fiber bragg grating sensors for railway systems," in *Fiber Bragg Grating Sensors: Recent Advancements, Industrial Applications and Market Exploitation*: Bentham Science, 2011, pp. 197-271.

[18] T. Snyder, "Personal Communication," 2020.

[19] D. Cannon, K. O. Edel, S. Grassie, and K. Sawley, "Rail defects: an overview," *Fatigue & Fracture of Engineering Materials & Structures*, vol. 26, no. 10, pp. 865-886, 2003.

[20] P. Loveday, D. Ramatlo, and F. Burger, "Monitoring of rail track using guided wave ultrasound," in *19th World Conference on Non-Destructive Testing 2016 Monitoring*, 2016, pp. 1-8.

[21] R. J. Black, J. M. Costa, B. Moslehi, and V. Sotoudeh, "Broadband fiber Bragg grating interrogation for structural health monitoring," SAMPE Baltimore, Baltimore, 2015.

[22] V. Sotoudeh, R. J. Black, B. Moslehi, and P. Qiao, "Lamb wave-based damage detection of composite shells using high-speed fiber-optic sensing," in *SPIE Smart Structures + NDE*, San Diego, 2014: SPIE, 2014, p. Paper 42.